ELSEVIER

0309-1708(94)00010-7

Advances in Water Resources 17 (1994) 283–296

0309-1708/95/$09.50

Analytical solutions for one-dimensional colloid transport in saturated fractures

Assem Abdel-Salam & Constantinos V. Chrysikopoulos*

Department of Civil and Environmental Engineering, University of California, Irvine, California 92717-2175, USA

(Received 21 March 1994; accepted 3 August 1994)

Closed-form analytical solutions for colloid transport in single rock fractures with and without colloid penetration into the rock matrix are derived for constant concentration as well as constant flux boundary conditions. A single fracture is idealized as two semi-infinite parallel plates. It is assumed that colloidal particles undergo irreversible deposition onto fracture surfaces and may penetrate into the rock matrix, and deposit irreversibly onto rock matrix solid surfaces. The solutions are obtained by taking Laplace transforms to the governing transport equations and boundary conditions with respect to time and space. For the case of no colloid penetration into the rock matrix, the solutions are expressed in terms of exponentials and complimentary error functions; whereas, for the case of colloid penetration into the rock matrix, the solutions are expressed in terms of convolution integrals and modified Bessel functions. The impact of the model parameters on colloid transport is examined. The results from several simulations indicate that liquid-phase as well as deposited colloid concentrations in the fracture are sensitive to the fracture surface deposition coefficient, the fracture aperture, and the Brownian diffusion coefficient for colloidal particles penetrating the rock matrix. Furthermore, it is shown that the differences between the two boundary conditions investigated are minimized at dominant advective transport conditions. The constant concentration condition overestimates liquid-phase colloid concentrations, whereas the constant flux condition leads to conservation of mass.

Key words: fractures, rock matrix, colloid transport, colloid deposition, analytical solutions.

NOMENCLATURE

b	Fracture aperture, L
d_p	Colloidal particle diameter, L
D	Dispersion coefficient for colloids, L^2/T
$\mathscr{D}_b$	Brownian diffusion coefficient for colloids, L^2/T
$\mathscr{D}_e$	Effective diffusion coefficient for colloids, L^2/T
erf[x]	Error function, equal to $2\pi^{-1/2}\int_0^x e^{-z^2}dz$
erfc[x]	Complimentary error function, equal to $1 - \text{erf}[x]$
k	Boltzmann constant ($1{\cdot}38 \times 10^{-23}$ J/K), ML^2/KT^2
L^{-1}	Laplace inverse operator
n	Liquid-phase colloid concentration in the fracture, M/L^3
n_m	Liquid-phase colloid concentration in the rock matrix, M/L^3
n_0	Source colloid concentration, M/L^3
n^*	Colloid concentration deposited on fracture surfaces, M/L^2
n_m^*	Colloid concentration deposited on rock matrix solid-surfaces, M/M
s	Laplace transform variable with respect to time
t	Time, T
$\mathscr{T}$	Absolute temperature
U	Average interstitial velocity in the fracture, L/T
x	Coordinate along the fracture axis, L
z	Coordinate perpendicular to the fracture axis, L
β	Defined in eqn (25)
γ	Laplace transform variable with respect to distance
ϵ	Relative mass balance error, defined in eqn (22)
η	Dummy integration variable
θ	Porosity of the rock matrix (liquid volume/rock matrix volume), L^3/L^3
κ	Fracture surface deposition coefficient, L

*To whom correspondence should be addressed.

κ_m Rock matrix deposition coefficient, 1/T
μ Fluid dynamic viscosity, M/LT
ν Dummy integration variable
ξ Defined in eqn (10)
ρ_b Bulk density of the rock matrix, M/L^3
τ Dummy integration variable
τ^* Rock matrix tortuosity
ω Dummy integration variable

Subscripts
cc constant concentration boundary condition without colloid penetration into the rock matrix
cc_p constant concentration boundary condition with colloid penetration into the rock matrix
cf constant flux boundary condition without colloid penetration into the rock matrix
cf_p constant flux boundary condition with colloid penetration into the rock matrix

INTRODUCTION

Transport of colloids in subsurface formations has increasingly captured the attention of many researchers, because of the potential impact of colloids in facilitating the transport of pollutants and toxic elements (e.g. Refs 27, 28, 32, 35 and 39). Traditionally, contaminant transport in rock fractured media has been modeled under the assumption that dissolved species may flow along with fluid phases present in the system, may sorb onto the immobile solid phase associated with fracture surfaces, and may diffuse into rock-matrix micro-fissures (e.g. Refs 2, 16, 20, 22 and 29). However, recent experimental and field studies indicate that contaminants can also migrate, adsorbed on the surface of colloid particles (e.g. Refs 8, 9, 10 and 38). This may suggest that colloids not only enhance the mobility of contaminants in fractures, they also inhibit the retardation and dilution of contaminants by restricting their sorption onto fracture surfaces and diffusion into the rock matrix.

Colloids are very fine particles that range in size between 10^{-3} μm and 1 μm.[8] These particles may be introduced or formed in groundwater, for instance, as a result of well drilling, leaching from the vadose zone, and dissolution of inorganic cementing agents that bind colloidal-sized materials to solid surfaces.[26] Once a colloidal suspension is formed, it could be transported over significant lateral distances and thus facilitate contaminant movement. Suspended colloids are also subject to aggregation, filtration and settling, all of which are relatively complex processes dependent on colloid density, colloid size, surface chemistry, water chemistry, and interstitial velocity.[26]

The transport of colloids is affected by hydrodynamic interactions between colloidal particles, interstitial fluid, and fracture surfaces.[14] The stability of colloids is an important consideration in determining their transport and is controlled by van der Waals attractive forces that promote aggregation, and electrostatic repulsive forces that keep particles apart. When electrostatic repulsions are dominant, colloidal particles are electrostatically stabilized and remain in a dispersed state.[26] Conditions of weak electrostatic repulsive forces may promote coagulation which does not necessarily lead to immediate particle immobilization. Coagulation is a function of several variables, including particle concentration and particle size, which can influence the extent of particle–particle collisions. Moreover, destabilized colloids can still be transported as aggregates if the aggregates are sufficiently small relative to the fracture aperture.

As colloids are transported through fractures, a fracture is deposited onto fracture surfaces by physicochemical collection. Deposition of colloidal particles involves two processes: transport of particles from the bulk solution to the solid–liquid interface; and attachment of particles to the solid surface. The first process is associated with the collector efficiency, and represents the ratio of the rate at which particles strike the solid surface to the rate at which particles move toward the solid surface. The collector efficiency for submicron particles is primarily controlled by Brownian motion. The attachment of particles to the solid surface, or attachment efficiency, is the ratio of the rate at which particles attach to the solid surface to the rate at which particles strike the solid surface. The attachment efficiency is mainly affected by the repulsive electric double layer, the attractive van der Waals, and viscous interaction forces.[6,28,43] Particle deposition is also affected by particle shape, the solid surface roughness and whether the solid surface is clean or deposition is on previously collected particles.

Colloid transport and attachment onto solid surfaces are not independent processes. Therefore, it is customary to represent mathematically particle deposition by an empirical coefficient (filter or deposition coefficient), which is considered as an irreversible adsorption term accounting for the mechanisms governing the colloid deposition process. The DLVO (Deryaguin, Landau, Verwey, and Overbeek) theory is not in agreement with observed particle deposition rates particularly for negatively charged particles and solid surfaces.[6] Moreover, because the deposition coefficient depends on the absolute temperature, the density and viscosity of the aqueous-phase, the average particle size, and other parameters accounting for the electric double layer and van der Waals forces, it is usually determined from laboratory columns or field experimental measurements (e.g. Refs 9 and 38).

Deposited colloids are not expected to desorb from fracture surfaces. The rate of release of deposited colloids from smooth parallel-plate channels was experimentally found to be negligible.[6] Also, under the range of velocities encountered in crystalline rocks,

detachment of colloids is not likely to occur. Some studies of colloid transport in fractures suggest that colloids do not penetrate into certain types of rock matrices (e.g. Refs 6 and 7). For instance, Bradbury and Green[7] reported that particles in the size range of 0·091–0·312 μm can not penetrate a crystalline rock matrix with 0·14 μm micro-fissures. Since the size of colloids ranges between 10^{-3} and 1 μm, and the size of rock-matrix micro-fissures ranges between 0·01 and 10 μm[5], the possibility of colloids diffusing into the rock matrix cannot be eliminated.

Several modeling efforts have been conducted in the recent years on colloid and colloid-facilitated contaminant transport in subsurface environments. For instance, Harvey and Garabedian[17] developed a model based on the colloid-filtration theory for the transport of bacteria in a contaminated sandy aquifer. Mills *et al.*[28] presented a model to evaluate the significance of colloids on the mobility of metals in porous media. Hwang *et al.*[19] presented a model for colloid migration in a single planar fracture for the case where colloids do not deposit onto fracture surfaces. Grindrod[15] modeled the dispersal of a radioactive material in the presence of colloids in a single fracture. Abdel-Salam and Chrysikopoulos[1] developed a numerical model for the cotransport of contaminants and colloids in a fracture with nonlinear contaminant sorption onto colloids.

In any modeling process, boundary conditions are important because they account for effects of the system outside the region of interest. Usually, contaminant transport models assume that mass is introduced to the system through either a constant concentration (first-type or Dirichlet) or a constant flux (third-type or Cauchy) inlet boundary condition.[41] The constant concentration boundary condition represents the case where colloids exist at the inlet boundary at a prescribed constant concentration, while the constant flux boundary condition represents the case where colloids are added at a constant rate to the fluid that enters the fracture. The constant concentration boundary condition indicates that the advective flux across the boundary is constant, while the constant flux indicates that the sum of advective flux and the dispersive flux is constant. Solutions resulting from both boundary conditions can be used in the analysis of experimental breakthrough curves obtained by injecting colloids into a rock fracture.

The focus of this work is to derive analytical solutions for one-dimensional macroscopic colloid transport in a semi-infinite fracture accounting for irreversible deposition onto fracture surfaces, penetration into the rock matrix, and irreversible deposition onto rock-matrix solid surfaces. The fracture is conceptualized as two parallel plates. The solutions are developed for constant concentration as well as constant flux inlet boundary conditions. In the first part of this paper, solutions for the simpler case of colloid transport without colloid penetration into the rock matrix are derived. In the second part, solutions for the transport of colloids with penetration into the rock matrix are developed.

DEVELOPMENT OF MODELS

The partial differential equation governing colloid transport in a one-dimensional fracture idealized as two parallel plates (as shown in Fig. 1) under steady-state flow conditions, assuming that colloids may deposit irreversibly onto fracture surfaces, and may penetrate the rock matrix has been derived from mass balance considerations and can be written as

$$\frac{\partial n(t,x)}{\partial t}+\frac{2}{b}\frac{\partial n^*(t,x)}{\partial t}=D\frac{\partial^2 n(t,x)}{\partial x^2}-U\frac{\partial n(t,x)}{\partial x}+\frac{2\theta\mathscr{D}_e}{b}\frac{\partial n_m(t,x)}{\partial z}\bigg|_{z=b/2} \quad (1)$$

where n is the liquid-phase colloid concentration in the fracture; x is a coordinate along the fracture axis; t is time; z is a coordinate perpendicular to the fracture axis measured from the center of the fracture (see Fig. 1); D is the dispersion coefficient for colloids; U is the average interstitial velocity in the fracture; b is the fracture aperture bounded by the two fracture surfaces; n^* is the concentration of colloids retained by deposition onto fracture surfaces expressed as mass of colloids per unit area of fracture surface; θ is the porosity of the rock matrix; $\mathscr{D}_e=\mathscr{D}_b/\tau^*$ is the effective diffusion coefficient for colloids, $\mathscr{D}_b$ is the Brownian diffusion coefficient and τ^* is the rock matrix tortuosity ($\tau^*>1$);[4] and n_m is the colloid concentration in the rock matrix.

At certain conditions the dispersion coefficient of colloids is probably different than that of a dissolved contaminant. At the microscale, dispersion of colloids or a dissolved contaminant is caused mainly by Brownian diffusion and Taylor dispersion resulting from the parabolic velocity variations between the fracture surfaces.[21] In real rock fractures, macroscopic

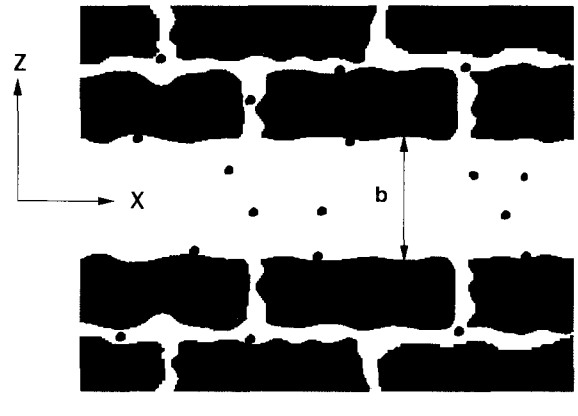

Fig. 1. Idealization of a natural fracture as two parallel plates surrounded by the rock matrix. The fracture has a mean aperture b.

dispersion is affected by fracture surface heterogeneities caused, for instance, by roughness perturbations and filling material. Macroscopically, in porous and fractured media, particularly at high Peclet number, dispersion of colloids and dissolved contaminants is expected to be independent of Brownian diffusion and consequently a single value of dispersivity should be valid for both colloids and dissolved contaminants.[21,30] Grindrod[15] used a macroscopic dispersion coefficient for dissolved contaminants which is 3.8 times larger than that of colloids. However, Smith and Degueldre[34] used a 1·5 times larger macroscopic dispersion coefficient for colloids. In this paper, the dispersion coefficient employed represents a macroscopic scale.

The second term on the left hand side of eqn (1) represents the mass flux of colloids onto fracture surfaces. At the microscale, interaction of colloids with fracture surfaces is affected by a variety of physicochemical mechanisms that control the deposition and transport of colloids; however, at the macroscale, colloid transport is modeled with a lumped deposition coefficient, which for the case of irreversible colloid deposition can be expressed as

$$\frac{\partial n^*(t,x)}{\partial t} = \frac{\kappa U}{b} n(t,x) \tag{2}$$

where κ is the fracture surface deposition coefficient, which is an experimentally determined 'lumped' parameter that takes into account the different deposition mechanisms induced by Brownian motion, van der Waals and electric double layer forces. This relationship assumes that n^* is not affected by previously deposited particles on fracture surfaces. A more realistic treatment for colloid deposition could be to include the effects of previously deposited particles; however, this approach will make the mathematical model nonlinear precluding an analytical solution. Similar relationships to eqn (2) for the filtration of colloids in porous media have been presented by Herzig *et al.*,[18] and Harvey and Garabedian;[17] and in fractured media by Bowen and Epstein.[6]

The last term in eqn (1) represents the diffusive mass flux of colloids into the rock matrix. The colloid concentration in the rock matrix, n_m, can be obtained from the following one-dimensional partial differential equation governing colloid diffusion in a direction perpendicular to the fracture axis, assuming that the interstitial liquid in the rock matrix is stationary, and that colloids deposit irreversibly onto rock-matrix solid surfaces

$$\frac{\partial n_m(t,x,z)}{\partial t} + \frac{\rho_b}{\theta}\frac{\partial n_m^*(t,x,z)}{\partial t} = \mathscr{D}_e \frac{\partial^2 n_m(t,x,z)}{\partial z^2} \tag{3}$$

where n_m^* is the colloid concentration deposited on the rock matrix. Similar to colloid deposition onto fracture surfaces (eqn (2)), the irreversible deposition of colloids onto rock-matrix solid surfaces can be expressed by the following linear kinetic relationship

$$\frac{\partial n_m^*(t,x,z)}{\partial t} = \frac{\kappa_m \theta}{\rho_b} n_m(t,x,z) \tag{4}$$

where κ_m is the rock matrix deposition coefficient. For a semi-infinite fracture and the presence of a continuous source of colloids, the initial and boundary conditions examined in this work are

$$n(0,x) = 0 \tag{5}$$

$$n(t,0) = n_0 \tag{6a}$$

$$-D\frac{\partial n(t,0)}{\partial x} + Un(t,0) = Un_0 \tag{6b}$$

$$\frac{\partial n(t,\infty)}{\partial x} = 0 \tag{7}$$

$$n_m(0,x,z) = 0 \tag{8a}$$

$$n_m(t,x,b/2) = n(t,x) \tag{8b}$$

$$\frac{\partial n_m(t,x,\infty)}{\partial z} = 0 \tag{8c}$$

where n_0 is the source colloid concentration. The condition (5) corresponds to the situation where colloids are initially absent from the one-dimensional fracture. The boundary condition (6a) represents the case of constant concentration at the inlet; while, the constant flux boundary condition (6b) implies colloidal concentration discontinuity at the inlet. The downstream boundary condition (7) preserves concentration continuity for a semi-infinite fracture. The boundary condition (8b) implies equal concentration in the fracture and the rock matrix at the interface between them.

Without colloid penetration into the rock matrix

For the case of constant concentration boundary condition, and without colloid penetration into the rock matrix (i.e. $\partial n_m/\partial z = 0$), the analytical solution to eqns (1), (2), (5), (6a) and (7) is derived using Laplace transform techniques and is given as

$$n_{cc}(t,x) = \frac{n_0}{2}\left\{\exp\left[\frac{Ux}{2D}(1-\xi)\right]\operatorname{erfc}\left[\frac{x-Ut\xi}{2(Dt)^{1/2}}\right] + \exp\left[\frac{Ux}{2D}(1+\xi)\right]\operatorname{erfc}\left[\frac{x+Ut\xi}{2(Dt)^{1/2}}\right]\right\} \tag{9}$$

where

$$\xi = \left(1 + \frac{8\kappa D}{Ub^2}\right)^{1/2} \tag{10}$$

and the subscript cc indicates the use of the constant concentration upstream boundary condition. It should be noted that for the case of non-depositing colloidal transport, κ is set to zero in the preceding equation. For

the case of constant flux inlet boundary condition, and without colloid penetration into the rock matrix, the analytical solution for eqns (1), (2), (5), (6b) and (7) is also derived using Laplace transform techniques to yield

$$n_{cf}(t,x) = n_0\left\{\frac{1}{1+\xi}\exp\left[\frac{Ux}{2D}(1-\xi)\right]\operatorname{erfc}\left[\frac{x-Ut\xi}{2(Dt)^{1/2}}\right] + \frac{1}{1-\xi}\exp\left[\frac{Ux}{2D}(1+\xi)\right]\operatorname{erfc}\left[\frac{x+Ut\xi}{2(Dt)^{1/2}}\right] + \frac{Ub^2}{4D\kappa}\exp\left[\frac{Ux}{D}-\frac{2U\kappa t}{b^2}\right]\operatorname{erfc}\left[\frac{x+Ut}{2(Dt)^{1/2}}\right]\right\} \quad (\kappa > 0) \tag{11}$$

where the subscript cf indicates the use of the constant flux upstream boundary condition. Analytical solutions for a mathematically similar but physically different model to the colloid transport model without colloid penetration into the rock matrix can be found in van Genuchten.[40] It should be noted that the preceding expression is valid only for $\kappa > 0$ which corresponds to $\xi > 1$. For the case of non-depositing colloidal transport, the solution can be obtained directly from the work of Lindstrom *et al.*,[25] and Gershon and Nir[13]

$$n_{cf}(t,x) = \frac{n_0}{2}\left\{\operatorname{erfc}\left[\frac{x-Ut}{2(Dt)^{1/2}}\right] + \left(\frac{4U^2t}{\pi D}\right)\times\exp\left[-\frac{(x-Ut)^2}{4Dt}\right] - \left(1+\frac{Ux}{D}+\frac{U^2t}{D}\right)\times\exp\left[\frac{Ux}{D}\right]\operatorname{erfc}\left[\frac{x+Ut}{2(Dt)^{1/2}}\right]\right\} \quad (\kappa = 0) \tag{12}$$

Colloid penetration into the rock matrix

For the case of constant concentration inlet boundary condition, and with colloid penetration into the rock matrix (i.e. $\partial n_m/\partial z > 0$), the analytical solution to eqns (1)–(6a), (7) and (8) can be derived following the methods of Lindstrom and Boersma,[24] and Chrysikopoulos *et al.*[11] Taking Laplace transforms with respect to time variable t and space variable x, using the transformed boundary conditions and applying inverse transformations yields

$$n_{cc_p}(t,x) = \frac{n_0}{\pi^{1/2}}\exp[B]\int_\ell^\infty \exp\left[-\eta^2-\frac{Ex^2}{4D\eta^2}\right]\times\left\{\exp\left[-\frac{\kappa_m x^2}{4D\eta^2}-\frac{\kappa_m^{1/2}Ax^2}{4\eta^2}\right]\times\operatorname{erfc}\left[\frac{Ax^2}{8\eta^2T^{1/2}}-(\kappa_m T)^{1/2}\right] + \exp\left[-\frac{\kappa_m x^2}{4D\eta^2}+\frac{\kappa_m^{1/2}Ax^2}{4\eta^2}\right]\times\operatorname{erfc}\left[\frac{Ax^2}{8\eta^2T^{1/2}}+(\kappa_m T)^{1/2}\right]\right\}d\eta \tag{13}$$

where the subscript cc_p indicates the use of the constant concentration upstream boundary condition with penetration into the rock matrix,

$$A = \frac{2\theta\mathscr{D}_e^{1/2}}{bD} \tag{14a}$$

$$B = \frac{Ux}{2D} \tag{14b}$$

$$E = \frac{2\kappa U}{b^2}+\frac{U^2}{4D}-\kappa_m \tag{14c}$$

$$\ell = \frac{x}{2(Dt)^{1/2}} \tag{14d}$$

$$T = t-\frac{x^2}{4D\eta^2} \tag{14e}$$

and η is a dummy integration variable. For the case of constant flux inlet boundary condition and with colloid penetration into the rock matrix, eqns (1)–(5), and (6b)–(8) are solved analytically in a similar fashion to the constant concentration boundary condition, and the solution is given as (see Appendix)

$$\eta_{cf_p}(t,x) = \frac{n_0U}{2\pi D^{1/2}}\exp[B-\kappa_m t][f(t)*g(t)] \tag{15}$$

where the subscript cf_p indicates the use of the constant flux upstream boundary condition with penetration into the rock matrix; and $f*g$ is the convolution integral defined as

$$f(t)*g(t) = \int_0^t f(\tau)g(t-\tau)d\tau \tag{16}$$

where

$$f(t) = \int_\ell^\infty \exp\left[-\eta^2-\frac{Ex^2}{4D\eta^2}\right]\left\{\exp\left[\kappa_m T-\frac{\kappa_m^{1/2}Ax^2}{4\eta^2}\right]\times\operatorname{erfc}\left[\frac{Ax^2}{8\eta^2T^{1/2}}-(\kappa_m T)^{1/2}\right]+\exp\left[\kappa_m T+\frac{\kappa_m^{1/2}Ax^2}{4\eta^2}\right]\times\operatorname{erfc}\left[\frac{Ax^2}{8\eta^2T^{1/2}}+(\kappa_m T)^{1/2}\right]\right\}d\eta \tag{17}$$

$$g(t) = \frac{1}{t^{3/2}}\left\{\int_0^\infty \exp\left[-\frac{\omega^2}{4t}-\omega(F+H)\right]\omega\,d\omega - P^{1/2}\int_0^\infty\int_0^\omega \exp\left[-\frac{\omega^2}{4t}-H\omega-F(\omega^2-\nu^2)^{1/2}\right]\times J_1[\nu P^{1/2}]\omega\,d\nu\,d\omega\right\} \tag{18}$$

$$F = \frac{U}{2D^{1/2}} \tag{19a}$$

$$H = \frac{AD}{2} \tag{19b}$$

$$P = E - \frac{A^2D^2}{4} \tag{19c}$$

τ, ν, and ω are dummy integration variables; and J_1 is the modified Bessel function of the first kind of order one.

MODELS SIMULATIONS AND DISCUSSION

Transport without penetration into the rock matrix

To illustrate the effect of the colloid transport model parameters, temporal and spatial distributions of colloids in the fracture have been calculated for a variety of situations for both the boundary conditions examined in case where $\partial n_m/\partial z = 0$. For simplicity, only the results for the constant flux boundary condition are presented, and the differences between the two boundary conditions are discussed briefly. For presentation purposes, the calculated colloid concentrations are normalized by the source colloid concentration. Unless otherwise specified, breakthrough curves are predicted at a distance $x = 5$ m downstream of the source, whereas snapshots are given at $t = 5y$; and the interstitial velocity is set at $U = 1$ m/year. The parameter values used are obtained from the work of Bowen and Epstein,[6] Abelin,[2] and Toran and Palumbo.[38]

The effect of the ratio of the fracture surface deposition coefficient, κ, to the fracture aperture squared, b^2, on the variation of the liquid-phase colloid concentration in the fracture with time and distance is shown in Fig. 2. The breakthrough curves (Fig. 2(a)) as well as the snapshots (Fig. 2(b)) presented, show that increasing the deposition coefficient, while holding the fracture aperture constant, results in a reduction in the liquid-phase colloid concentration. This result is expected since the deposition coefficient determines the amount of colloids to be deposited onto fracture surfaces. Figure 2 also shows that, by holding the deposition coefficient constant, the liquid-phase colloid concentration decreases with decreasing fracture aperture. This result is attributable to the fact that the smaller the fracture aperture the easier the access of colloidal particles to fracture surfaces due to the shorter distance to be traveled. It should be noted that the effect of an increase in the fracture aperture is exactly opposite to the effect of an increase in the deposition coefficient. Furthermore, in Fig. 2(a) the normalized concentrations of colloids in solution do not reach the maximum value of one, because irreversible and indefinite deposition onto fracture surfaces (i.e. a perfect sink) is assumed.

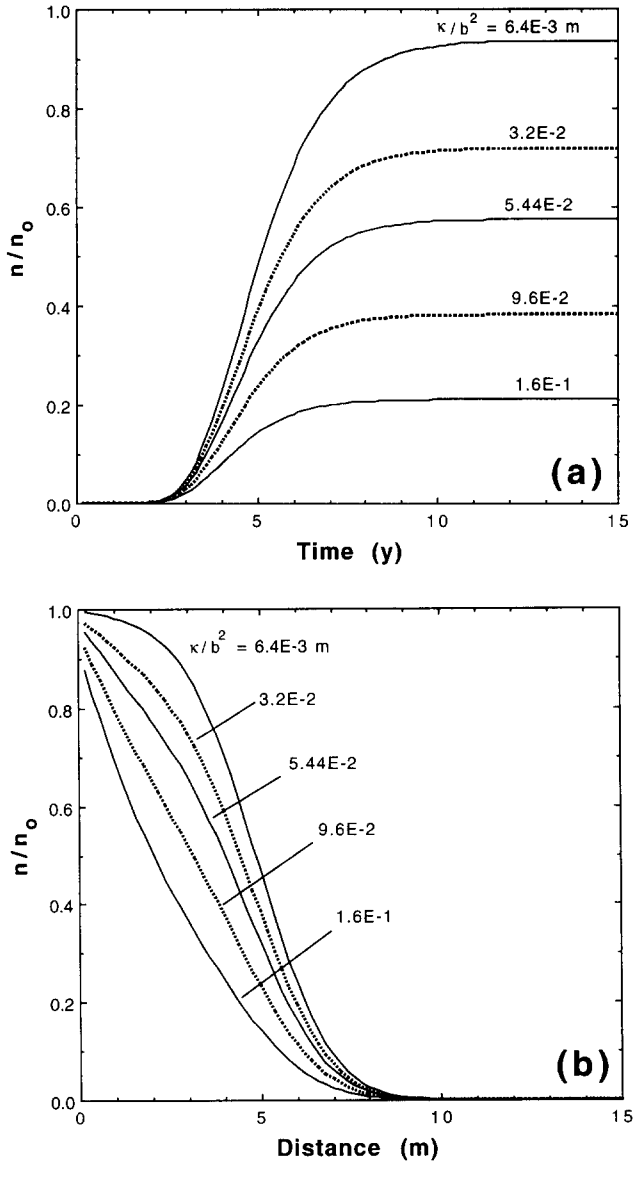

Fig. 2. Effect of the ratio of the fracture surface deposition coefficient to the fracture aperture squared on (a) temporal, and (b) spatial normalized liquid-phase colloid distribution in the fracture ($D = 0{\cdot}25\,m^2$/year, and $U = 1{\cdot}0$ m/year).

Maximum breakthrough concentrations are obtained for nondepositing colloids (i.e. $\kappa = 0$).

To illustrate the differences between the two boundary conditions considered in this study, simulated breakthrough curves as well as snapshots using eqns (9) and (11) for two different dispersion coefficients are shown in Fig. 3, and for several interstitial velocities are presented in Fig. 4. The discrepancies in the calculated colloid concentrations are more significant at high dispersion coefficients and low velocities. Since the boundary conditions (6a) and (6b) are approximately equivalent when D is negligible, the behavior of the analytical solutions (9) and (11) is similar at low dispersion coefficients. Furthermore, as the interstitial velocity increases the advective flux in (6b) dominates over the dispersive flux and thus there is no

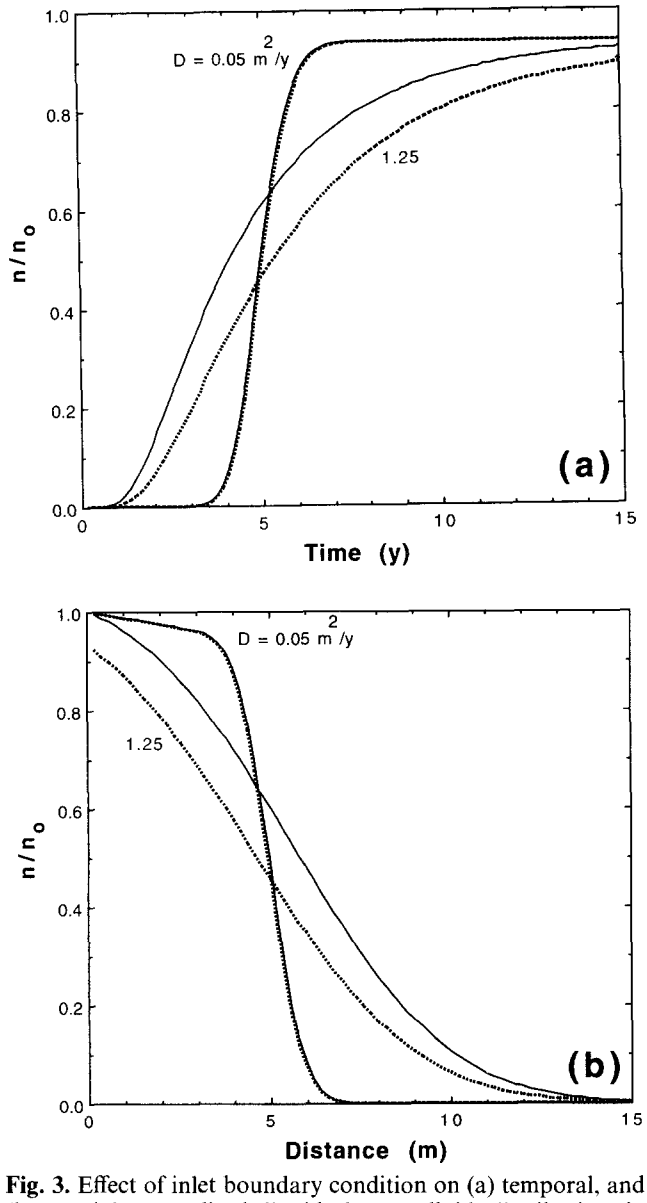

Fig. 3. Effect of inlet boundary condition on (a) temporal, and (b) spatial normalized liquid-phase colloid distribution in the fracture for different dispersion coefficients ($b = 1{\cdot}25 \times 10^{-4}$ m, $U = 1{\cdot}0$ m/year, and $\kappa = 1{\cdot}0 \times 10^{-10}$ m). Solid lines represent constant concentration and broken lines represent constant flux inlet boundary condition.

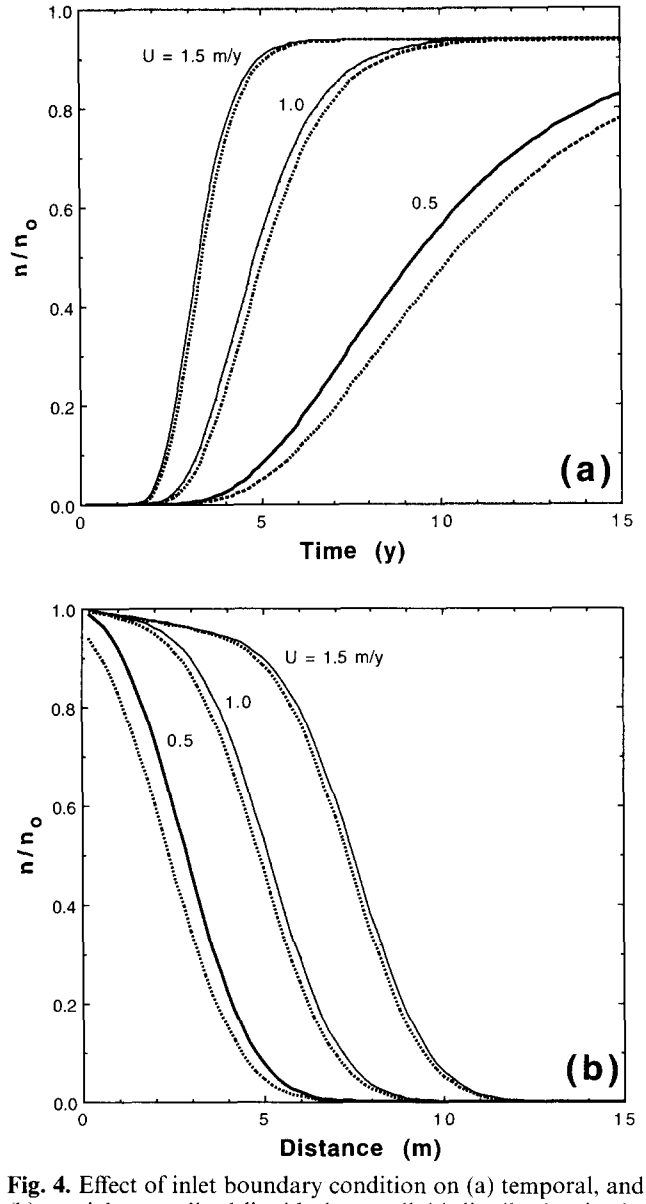

Fig. 4. Effect of inlet boundary condition on (a) temporal, and (b) spatial normalized liquid-phase colloid distribution in the fracture, for different velocities ($b = 1{\cdot}25 \times 10^{-4}$ m, $D = 0{\cdot}25\,\mathrm{m}^2$/year, and $\kappa = 1{\cdot}0 \times 10^{-10}$ m). Solid lines represent constant concentration and broken lines represent constant flux inlet boundary condition.

essential difference between the two boundary conditions, and consequently the two analytical solutions presented are equivalent. The colloidal concentration discontinuity at the inlet, imposed by the constant flux boundary condition, is illustrated in Figs 3(b) and 4(b), for the case of high dispersion and small velocity.

In addition to the simulations presented for the liquid-phase colloid concentration in the fracture, the effect of the transport parameters on the deposited colloid concentration on fracture surfaces is also examined. In view of eqn (2) it is evident that the deposited colloid concentrations on fracture surfaces for constant concentration and constant flux inlet boundary conditions are given by

$$n^*_{cc}(t,x) = \frac{\kappa U}{b}\int_0^t n_{cc}(\tau,x)\mathrm{d}\tau \tag{20}$$

$$n^*_{cf}(t,x) = \frac{\kappa U}{b}\int_0^t n_{cf}(\tau,x)\mathrm{d}\tau \tag{21}$$

respectively, where $n_{cc}(t,x)$ and $n_{cf}(t,x)$ are given by eqns (9) and (11), respectively. Since analytical evaluation of the integrals in eqns (20) and (21) is not straightforward, numerical integration by the extended Simpson's rule is applied.[31] Figure 5 shows predicted n^*_{cf} concentrations normalized by n_0, as a function of time and space for three different dispersion coefficients. Similar to the case of the liquid-phase colloid concen-

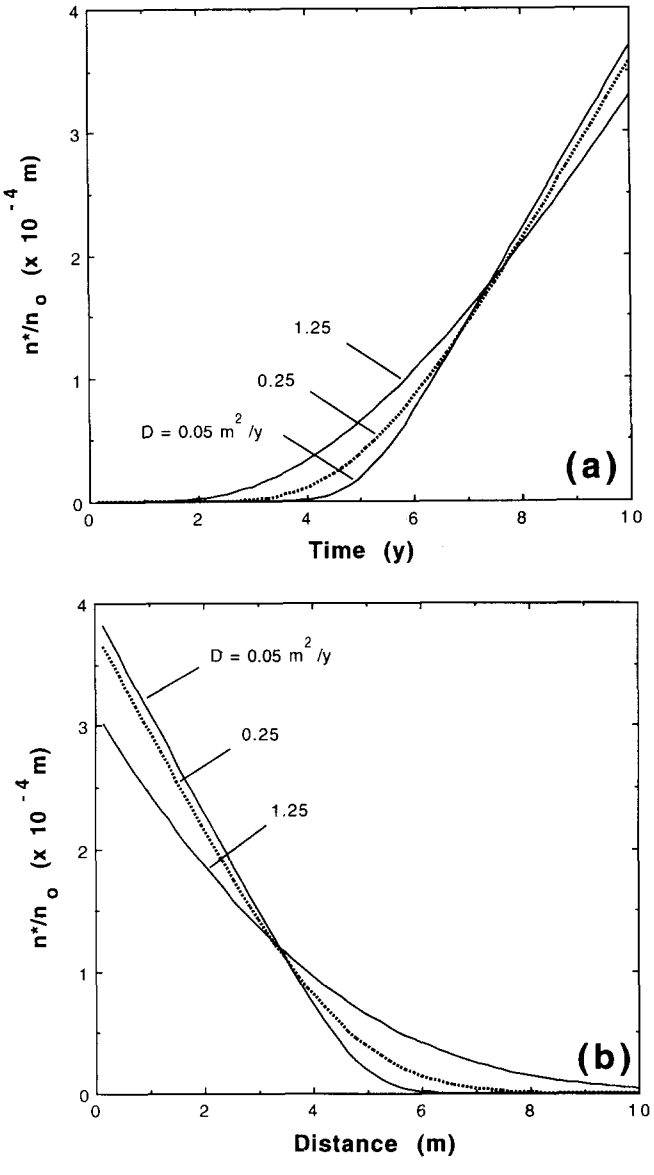

Fig. 5. Effect of dispersion coefficient on (a) temporal, and (b) spatial normalized deposited colloid distribution on fracture surfaces ($b = 1{\cdot}25 \times 10^{-4}$ m, $U = 1{\cdot}0$ m/year, and $\kappa = 1{\cdot}0 \times 10^{-10}$ m).

tration (Fig. 3), the deposited colloid concentration and the required time to steady state increases with increasing dispersion coefficient. The gradient of the deposited colloid concentration with respect to time is proportional to the liquid-phase colloid concentration (see eqn (2)); therefore, $\partial n^*(t,x)/\partial t$ becomes constant at steady state. Furthermore, Fig. 5(b) illustrates that deposited colloids spread over a greater portion of fracture surfaces at higher dispersion coefficients.

Mass balance errors

Previous investigations[3,23,42] suggest that improper use of boundary conditions may lead to conservation of mass errors. Following the work of van Genuchten and Parker[42] and assuming that the total mass flux of colloids entering the system corresponds to a constant flux, the relative mass balance error for colloids can be defined as

$$\epsilon = \epsilon_n + \epsilon_{n^*} - 1 = \frac{1}{Un_0 t}\int_0^\infty n(t,x)\,dx + \frac{1}{Un_0 tb}\int_0^\infty n^*(t,x)\,dx - 1 \tag{22}$$

where ϵ is the relative mass balance error, the term $Un_0 t$ is the mass of colloids entering the fracture at the inlet boundary over the time period t, and the integrals on the right hand side of the preceding equation represent the mass of colloids in the liquid-phase and deposited onto fracture surfaces, respectively, present in the fracture at time t. In view of eqn (22), the integral expressions of the liquid-phase colloid concentration $n(t,x)$ for constant concentration (9) and constant flux (11) boundary conditions can be written as

$$\epsilon_{n_{cc}} = \frac{\exp[\beta(1-\xi^2)]\,\mathrm{erfc}[-\beta^{1/2}] + \xi\,\mathrm{erfc}[\beta^{1/2}]}{2\beta(1-\xi^2)} - \frac{1}{2\beta(1-\xi)} \tag{23}$$

$$\epsilon_{n_{cf}} = \frac{\exp[\beta(1-\xi^2)]\,\mathrm{erfc}[-\beta^{1/2}] - 1}{\beta(1-\xi^2)} + \frac{b^2}{2\kappa tU}\exp\left[\frac{-2\kappa tU}{b^2}\right]\mathrm{erf}[\beta^{1/2}] \tag{24}$$

where

$$\beta = \frac{U^2 t}{4D} \tag{25}$$

In view of eqns (20), (21) and (22), the double integral expressions of the deposited colloid concentration for both boundary conditions ($\epsilon_{n^*_{cc}}, \epsilon_{n^*cf}$) are obtained numerically by the extended Simpson's rule.[31] The total relative mass balance error for the two boundary conditions is plotted as a function of the dispersion coefficient (Fig. 6(a)) and interstitial velocity (Fig. 6(b)). These figures indicate that the relative error for the constant concentration boundary condition is minimized at small dispersions and high velocities. Similar mass balance error trends have been obtained by van Genuchten and Parker,[42] and Leij *et al.*[23] for certain cases of solute transport in porous media. It should be noted that the constant concentration inlet boundary condition overestimates the liquid-phase colloid concentration, whereas the constant flux leads to conservation of mass.

Transport with penetration into the rock matrix

In this section, we investigate the impact of the model parameters controlling the mass flux of colloids into the rock matrix on the liquid-phase colloid concentration in the fracture. The analytical solutions to the colloid

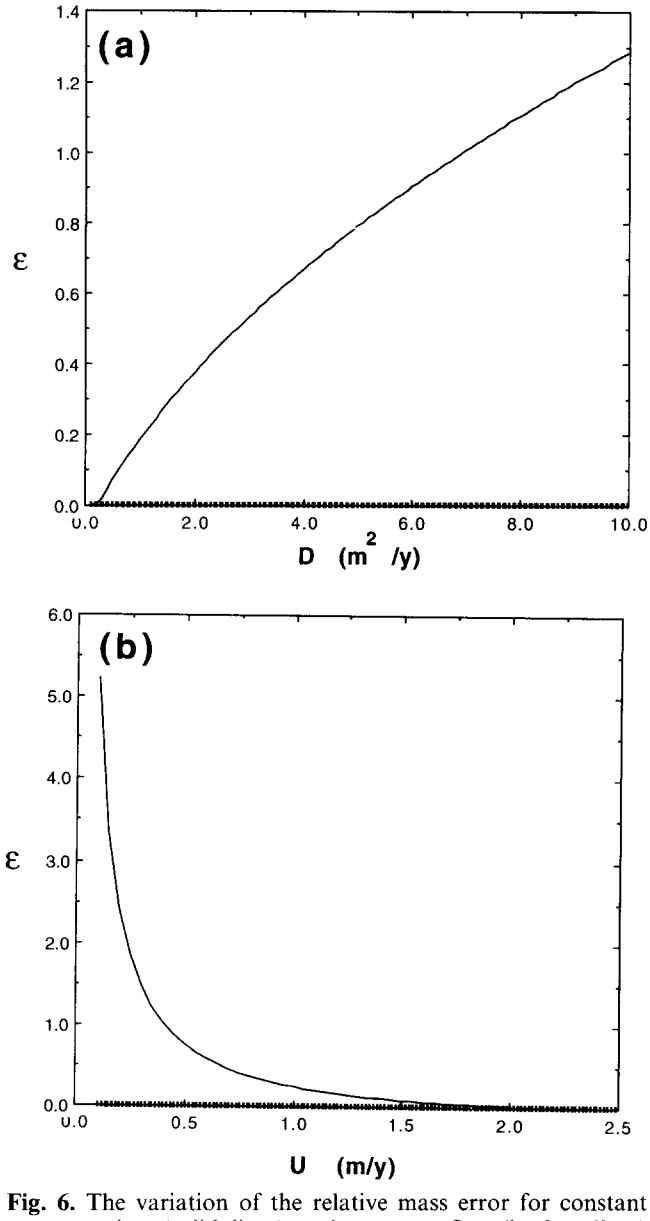

Fig. 6. The variation of the relative mass error for constant concentration (solid lines) and constant flux (broken lines) boundary conditions with (a) dispersion coefficient, and (b) interstitial velocity ($b = 1{\cdot}25 \times 10^{-4}$ m, and $\kappa = 1{\cdot}0 \times 10^{-9}$ m).

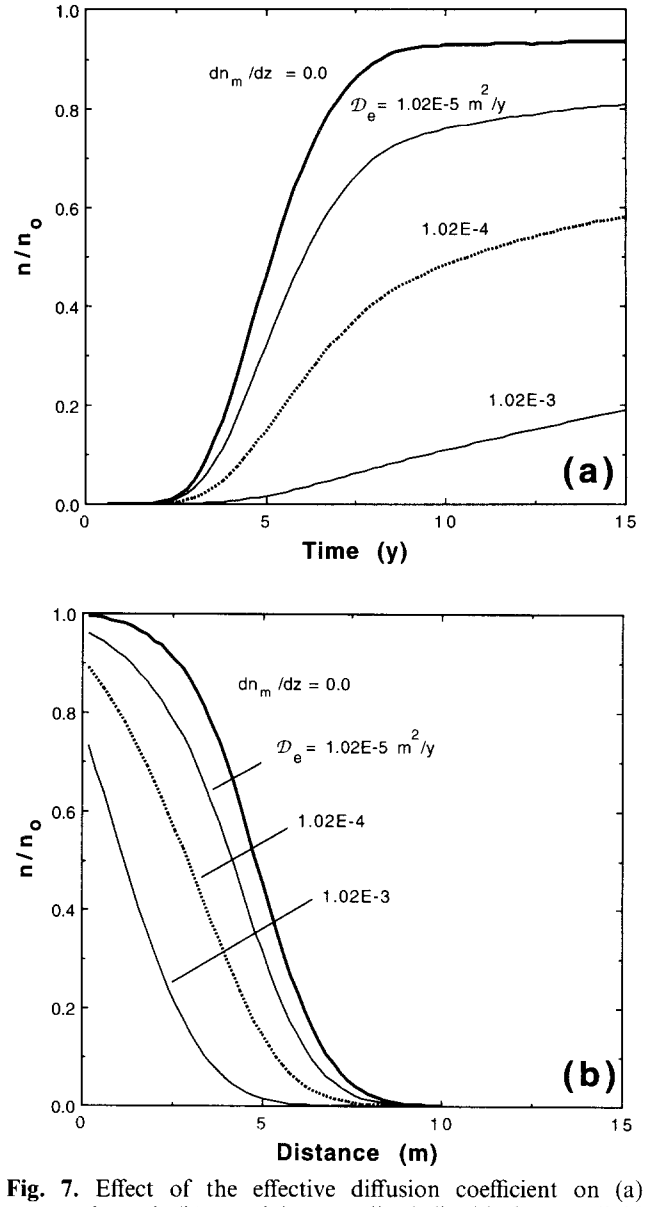

Fig. 7. Effect of the effective diffusion coefficient on (a) temporal, and (b) spatial normalized liquid-phase colloid distribution in the fracture ($b = 1{\cdot}25 \times 10^{-4}$ m, $D = 0{\cdot}25\,\mathrm{m}^2$/year, $U = 1{\cdot}0$ m/year, $\kappa = 1{\cdot}0 \times 10^{-10}$ m, and $\kappa_m = 0$/year).

transport model with penetration into the rock matrix for constant concentration and constant flux inlet boundary conditions are given by eqns (13) and (15), respectively. The integrals in these two solutions are not easily obtained analytically, and consequently they are evaluated using the Romberg numerical integration subroutine QROMO from Press *et al.*[31] The simulations using solutions (13) and (15) for $\partial n_m/\partial z = 0$ are compared with the simpler solutions (9) and (11) for the case where colloids do not penetrate into the rock matrix, and excellent agreement is found. For presentation purposes, only results from the constant flux boundary condition solution (eqn (15)) are presented. Breakthrough curves are predicted at $x = 5$ m, whereas snapshots are given at $t = 5y$; and the interstitial velocity is $U = 1$ m/year.

One of the parameters that appears in the diffusive mass flux term in the governing transport equation (1) is the effective diffusion coefficient for colloids. The Brownian diffusion coefficient is estimated by[12]

$$\mathscr{D}_b = \frac{k\mathscr{T}}{3\pi\mu d_p} \tag{26}$$

where k is the Boltzmann constant ($1{\cdot}38 \times 10^{-23}$ J/K); $\mathscr{T}$ is the absolute temperature; μ is the fluid dynamic viscosity; and d_p is the colloidal particle diameter. For colloids with particle diameter of $1{\cdot}0\,\mu$m at 20°C, the coefficient $\mathscr{D}_b$ is estimated by eqn (26) to be $1{\cdot}36 \times 10^{-5}\,\mathrm{m}^2$/year. The impact of the effective diffusion coefficient for colloids on the liquid-phase colloid concentration in the fracture is shown in Fig. 7. Three different effective diffusion coefficients are used in the

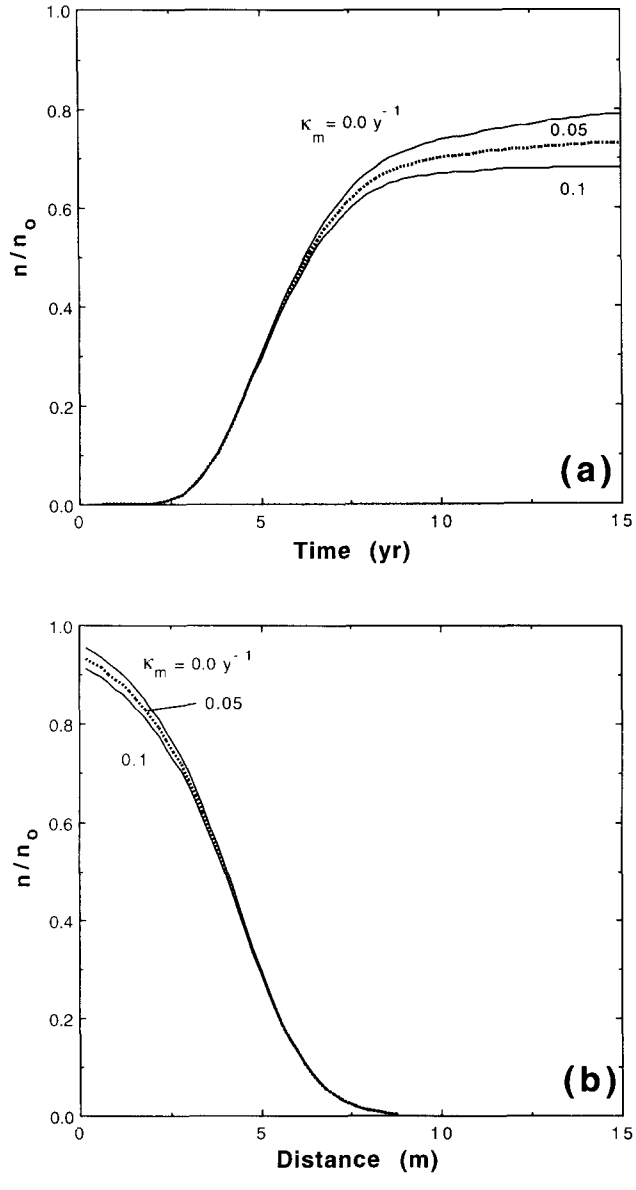

Fig. 8. Effect of the rock matrix deposition coefficient on (a) temporal, and (b) spatial normalized liquid-phase colloid distribution in the fracture ($b = 1{\cdot}25 \times 10^{-4}$ m, $D = 0{\cdot}25\,m^2$/year, $U = 1{\cdot}0$ m/year, $\mathscr{D}_e = 1{\cdot}02 \times 10^{-5}\,m^2$/year, and $\kappa = 1{\cdot}0 \times 10^{-10}$ m).

simulations corresponding to colloidal particle diameters of 1, 0·1, and 0·01 μm, and tortuosity τ^* of 1·33. The upper most curve in Fig. 7 corresponds to colloid transport without colloid penetration into the rock matrix. Predicted breakthrough curves as well as snapshots in Fig. 7 clearly demonstrate that an increase in the effective diffusion coefficient, or alternatively a decrease in particle size, leads to an increase in the colloidal mass flux into the rock matrix and consequently a decrease in the liquid-phase colloid concentration in the fracture. Figure 7(a) also shows that colloidal breakthrough time increases with increasing effective diffusion coefficient.

The impact of the rock matrix deposition coefficient on the liquid-phase colloid concentration in the fracture is demonstrated in Fig. 8. An increase in the rock matrix deposition coefficient (κ_m), leads to a decrease in the colloid concentration in the rock matrix (n_m). Consequently, the concentration gradient between the liquid-phase colloids in the fracture (n) and n_m increases leading to higher colloidal mass flux into the rock matrix. Figure 8 clearly shows this effect, although the liquid-phase colloid concentration in the fracture is not as sensitive to κ_m as it is to $\mathscr{D}_e$.

SUMMARY AND CONCLUSIONS

One-dimensional colloid transport in a single semi-infinite fracture idealized as two parallel plates was modeled assuming irreversible deposition onto fracture surfaces, penetration into the rock matrix, and irreversible deposition onto rock-matrix solid surfaces. Several analytical solutions corresponding to colloid transport with and without penetration into the rock matrix were derived using Laplace transform techniques, for constant concentration as well as constant flux inlet boundary conditions. Also, expressions for the concentration of deposited colloids onto fracture surfaces were provided.

The effect of the different parameters on the behavior of the model was investigated. The liquid-phase colloid concentration in the fracture was found to be mostly sensitive to the fracture aperture and to the fracture surface deposition coefficient. An increase in the deposition coefficient produces an increase in the deposited colloid concentration on fracture surfaces and consequently a decrease in the liquid-phase colloid concentration. As the fracture aperture decreases the liquid-phase colloid concentration declines sharply, while the deposited colloid concentration on fracture surfaces increases. The normalized steady state liquid-phase colloid concentration in the fracture does not reach the maximum value of one, because of the irreversible colloid deposition onto fracture surfaces.

It was shown that mass balance errors arise for the constant concentration inlet boundary condition, because this condition assumes that the colloid mass entering the system is solely by advection, in comparison to the constant flux inlet boundary condition which accounts for mass entering by advection as well as by dispersion. When the total mass flux is dominated by the advective mass flux (i.e. at low dispersion and/or high velocity), both boundary conditions yield similar concentration profiles. However, the constant concentration inlet boundary condition consistently overestimates the liquid-phase colloid concentrations.

Simulations of the analytical solutions for the case where colloids penetrate the rock matrix indicate an increase in the colloidal mass flux penetrating the rock matrix with decreasing particle size, which in turn leads to a reduction in the liquid-phase colloid concentration

in the fracture. The model was found to be relatively insensitive to the rock matrix deposition coefficient.

Although the models presented here have advantages due to their analytical nature, some of the limitations inherent to the models are their inability: (a) to allow for colloid deposition rates as a slowly varying function of colloid surface coverage; and (b) to account for variability in the aperture which is always present in real rock fractures. Nonetheless, these models can provide means for verifying the accuracy of numerical solutions to more comprehensive models for colloid transport in fractured subsurface formations.

REFERENCES

1. Abdel-Salam, A. & Chrysikopoulos, C. V. Analysis of a model for contaminant transport in fractured media in the presence of colloids. *J. Hydrol.* (in press).
2. Abelin, H. Migration in a single fracture: An in-situ experiment in a natural fracture. Ph.D. dissertation, Dep. of Chem. Eng., R. Inst. of Tech., Stockholm, Sweden, 1986, 170 pp.
3. Batu, V. & van Genuchten, M. Th. First- and third-type boundary conditions in two dimensional solute transport modeling. *Water Resour. Res.*, **26**(2) (1990) 339–50.
4. Bear, J. *Dynamics of Fluids in Porous Media.* Elsevier, 1972, 764 pp.
5. Birgersson, L. & Neretnieks, I. Diffusion in the Matrix of Granitic Rock Field Test in the Stripa Mine. Part 1. SKBF/KBS Teknish Rapport, 82-08, Royal Inst. of Technol., Stockholm, Sweden, 1982.
6. Bowen, B. D. & Epstein, N. Fine particle deposition in smooth parallel-plate channels. *J. Colloid Interface Sci.*, **72**(1) (1979) 81–97.
7. Bradbury, M. H. & Green, A. Investigations into the factors influencing long range matrix diffusion rates and pore space accessibility at depth in granite. *J. Hydrol.*, **89** (1986) 123–39.
8. Buddemeier, R. W. & Hunt, J. R. Transport of colloidal contaminants in groundwater radionuclide migration at the Nevada test site. *Appl. Geochem.*, **3** (1988) 535–48.
9. Champ, D. R. & Schroeter, J. Bacterial transport in fractured rock: A field-scale tracer test at the Chalk River Nuclear Laboratories. *Water Sci. Technol.*, **20**(11/12) (1988) 81–7.
10. Chiou, C. T., Malcolm, R. L., Brinton, T. I. & Kile, D. E. Water solubility enhancement of some organic pollutants and pesticides by dissolved humic and fulvic acids. *Environ. Sci. Technol.*, **20**(5) (1986) 502–8.
11. Chrysikopoulos, C. V., Roberts, P. V. & Kitanidis, P. K. One-dimensional solute transport in porous media with partial well-to-well recirculation: Application to field experiments. *Water Resour. Res.*, **26**(6) (1990) 1189–95.
12. Einstein, A. *Investigations on the Theory of the Brownian Movement*, ed. R. Furth, Dover, Mineola, NY, 1956.
13. Gershon, N. D. & Nir, A. Effects of boundary conditions of models on tracer distribution in flow through porous mediums. *Water Resour. Res.*, **5**(4) (1969) 830–9.
14. Goldman, A. J., Cox, R. G. & Brenner, H. Slow viscous motion of a sphere parallel to a plane wall — I: Motion through quiescent fluid. *Chem. Engng Sci.*, **22** (1967) 637–51.
15. Grindrod, P. The impact of colloids on the migration and dispersal of radionuclides within fractured rock. *J. Contam. Hydrol.*, **13** (1993) 167–81.
16. Haldeman, W. R., Chuang, Y., Rasmussen, T. C. & Evans, D. D. Laboratory analysis of fluid flow and solute transport through a fracture embedded in porous tuff. *Water Resour. Res.*, **27**(1) (1991) 53–65.
17. Harvey, R. W. & Garabedian, S. P. Use of colloid filtration theory in modeling movement of bacteria through a contaminated sandy aquifer. *Environ. Sci. Technol.*, **25** (1991) 178–85.
18. Herzig, J. P., Leclerc, D. M. & Le Goff, P. Flow of suspension through porous media: Application to deep filtration. *Ind. Engng Chem.*, **62**(5) (1970) 9–35.
19. Hwang, Y., Pigford, T. H., Lee, W. W. L. & Chambre, P. L. Analytic solution of pseudocolloid migration in fractured rock. *Mat. Res. Soc. Symp. Proc.*, **176** (1990) 599–605.
20. Johns, R. A. & Roberts, P. V. A solute transport model for channelized flow in a fracture. *Water Resour. Res.*, **27**(8) (1991) 1797–1808.
21. Kessler, J. H. & Hunt, J. R. Dissolved and colloidal contaminant transport in a partially clogged fracture. *Water Resour. Res.*, **30**(4) (1994) 1195–206.
22. Krishnamoorthy, T. M., Nair, R. N. & Sarma, T. P. Migration of radionuclides from a granite repository. *Water Resour. Res.*, **28**(7) (1992) 1927–34.
23. Leij, F. J., Skaggs, T. H. & van Genuchten, M. Th. Analytical solutions for solute transport in three-dimensional semi-infinite porous media. *Water Resour. Res.*, **27**(10) (1991) 2719–33.
24. Lindstrom, F. T. & Boersma, L. A theory on the mass transport of previously distributed chemicals in a water saturated sorbing porous medium. *Soil Sci.*, **111**(3) (1971) 192–9.
25. Lindstrom, F. T., Haque, R., Freed, V. H. & Boersma, L. Theory on the movement of some herbicides in soils: Linear diffusion and convection of chemicals in soils. *Environ. Sci. Technol.*, **1**(7) (1967) 561–5.
26. McCarthy, J. F. & Zachara, J. M. Subsurface transport of contaminants. *Environ. Sci. Technol.*, **23**(5) (1989) 496–502.
27. McDowell-Boyer, L. M., Hunt, J. R. & Sitar, N. Particle transport through porous media. *Water Resour. Res.*, **22**(13) (1986) 1901–21.
28. Mills, W. B., Liu, S. & Fong, F. K. Literature review and model (COMET) for colloid/metals transport in porous media. *Ground Water*, **29**(2) (1991) 199–208.
29. Moreno, L., Tsang, Y. W., Tsang, C. F., Hale, F. V. & Neretnieks, I. Flow and tracer transport in a single fracture: A stochastic model and its relation to some field observations. *Water Resour. Res.*, **24** (1988) 2033–48.
30. NAGRA, Project Gewahr. In Nuclear Waste Management in Switzerland: Feasibility Studies and Safety Analyses, Wettingen, Rep. NGB 85-05. Nat. Coop. Storage Radioactive Waste, Baden, Switzerland, 1985, 209 pp.
31. Press, W. H., Teukolsky, S. A., Vetterling, W. T. & Flannery, B. P. *Numerical Recipes: The Art of Scientific Computing*, Cambridge University Press, New York, 1992, 963 pp.
32. Puls, R. W. & Powell, R. M. Transport of inorganic colloids through natural aquifer material: Implications for contaminant transport. *Environ. Sci. Technol.*, **26** (1992) 614–21.
33. Roberts, G. E. & Kaufman, H. *Table of Laplace Transforms*, W. B. Saunders, Philadelphia, 1966, 367 pp.
34. Smith, P. A. & Degueldre, C. Colloid-facilitated transport of radionuclides through fractured media. *J. Contam. Hydrol.*, **13** (1993) 143–66.

35. Song, L. & Elimelech, M. Dynamics of colloid deposition in porous media: Modeling the role of retained particles. *Colloids and Surfaces A*, **73** (1993) 49–63.
36. Spiegel, M. R. *Laplace Transforms*, McGraw-Hill, 1990, 261 pp.
37. Tang, D. H., Frind, E. O. & Sudicky, E. A. Contaminant transport in fractured porous media: Analytical solution for a single fracture. *Water Resour. Res.*, **17**(3) (1981) 555–64.
38. Toran, L. & Palumbo, A. V. Colloid transport through fractured and unfractured laboratory sand columns. *J. Contam. Hydrol.*, **9** (1992) 289–303.
39. Torok, J., Buckley, L. P. & Woods, B. L. The separation of radionuclide migration by solution and particle transport in soil. *J. Contam. Hydrol.*, **6** (1990) 185–203.
40. van Genuchten, M. Th. Analytical solutions for chemical transport with simultaneous adsorption, zero-order production and first-order decay. *J. Hydrol.*, **49** (1981) 213–33.
41. van Genuchten, M. Th. & Alves, W. J. Analytical solutions of the one-dimensional convective–dispersive solute transport equation. US Department of Agriculture, Technical Bulletin No. 1661, 1982, 151 pp.
42. van Genuchten, M. Th. & Parker, J. C. Boundary conditions for displacement experiments through short laboratory soil columns. *Soil Sci. Soc. Am. J.*, **48** (1984) 703–8.
43. Yao, K. M., Habibian, M. T. & O'Melia, C. R. Water and waste water filtration: Concepts and applications. *Environ. Sci. Technol.*, **11** (1971) 1105–12.

APPENDIX: DERIVATION OF $n_{cf_p}(t,x)$

The desired function $n_{cf_p}(t,x)$ is the solution to the problem described by the following partial differential equations and initial/boundary conditions

$$\frac{\partial n(t,x)}{\partial t} = D\frac{\partial^2 n(t,x)}{\partial x^2} - U\frac{\partial n(t,x)}{\partial x} - \frac{2\kappa U}{b^2}n(t,x) + \frac{2\theta\mathscr{D}_e}{b}\frac{\partial n_m(t,x)}{\partial z}\bigg|_{z=b/2} \tag{A1}$$

$$\frac{\partial n_m(t,x,z)}{\partial t} = \mathscr{D}_e\frac{\partial^2 n_m(t,x,z)}{\partial z^2} - \kappa_m n_m(t,x,z) \tag{A2}$$

$$n(0,x) = 0 \tag{A3}$$

$$-D\frac{\partial n(t,0)}{\partial x} + Un(t,0) = Un_0 \tag{A4}$$

$$\frac{\partial n(t,\infty)}{\partial x} = 0 \tag{A5}$$

$$n_m(0,x,z) = 0 \tag{A6a}$$

$$n_m(t,x,b/2) = n(t,x) \tag{A6b}$$

$$\frac{\partial n_m(t,x,\infty)}{\partial z} = 0 \tag{A6c}$$

The solution is obtained with the methods of Lindstrom and Boersma,[24] and Chrysikopoulos *et al.*[11] Taking Laplace transforms with respect to the variable t of eqns (A1), (A2), and (A4)–(A6b, c) yields

$$[s\tilde{n}(s,x) - n(0,x)] = D\frac{\mathrm{d}^2\tilde{n}(s,x)}{\mathrm{d}x^2} - U\frac{\mathrm{d}\tilde{n}(s,x)}{\mathrm{d}x} - \frac{2\kappa U}{b^2}\tilde{n}(s,x) + \frac{2\theta\mathscr{D}_e}{b}\frac{\mathrm{d}\tilde{n}_m(s,x)}{\mathrm{d}z}\bigg|_{z=b/2} \tag{A7}$$

$$[s\tilde{n}_m(s,x,z) - n_m(0,x,z)] = \mathscr{D}_e\frac{\mathrm{d}^2\tilde{n}_m(s,x,z)}{\mathrm{d}z^2} - \kappa_m\tilde{n}_m(s,x,z) \tag{A8}$$

$$-D\frac{\mathrm{d}\tilde{n}(s,0)}{\mathrm{d}x} + U\tilde{n}(s,0) = \frac{Un_0}{s} \tag{A9}$$

$$\frac{\mathrm{d}\tilde{n}(s,\infty)}{\mathrm{d}x} = 0 \tag{A10}$$

$$\tilde{n}_m(s,x,b/2) = \tilde{n}(s,x) \tag{A11}$$

$$\frac{\mathrm{d}\tilde{n}_m(s,x,\infty)}{\mathrm{d}z} = 0 \tag{A12}$$

where the tilde signifies Laplace transform of t, and s is the transformed time variable. Substituting (A6a) into (A8) and solving the resulting second-order ordinary differential equation using the boundary conditions (A11) and (A12) and taking the derivative $\partial\tilde{n}_m/\mathrm{d}z$ evaluated at $z = b/2$ yields

$$\frac{\mathrm{d}\tilde{n}_m(s,x,b/2)}{\mathrm{d}z} = -\tilde{n}(s,x)\left[\frac{s+\kappa_m}{\mathscr{D}_e}\right]^{1/2} \tag{A13}$$

Employing (A3), and (A13) in (A7) and then taking Laplace transforms of the resulting equation with respect to space variable x leads to

$$s\hat{\tilde{n}}(s,\gamma) = D\left[\gamma^2\hat{\tilde{n}}(s,\gamma) - \gamma\tilde{n}(s,0) - \frac{\mathrm{d}\tilde{n}(s,0)}{\mathrm{d}x}\right] - U[\gamma\hat{\tilde{n}}(s,\gamma) - \tilde{n}(s,0)] - \frac{2\kappa U}{b^2}\hat{\tilde{n}}(s,\gamma) - \frac{2\theta[\mathscr{D}_e(s+\kappa_m)]^{1/2}}{b}\hat{\tilde{n}}(s,\gamma) \tag{A14}$$

where the hat signifies Laplace transform of x, and γ is the transformed space variable. Employing boundary condition (A9) into (A14) and solving for $\hat{\tilde{n}}(s,\gamma)$ following the procedure outlined in Chrysikopoulos *et al.*[11] results in

$$\hat{\tilde{n}}(s,\gamma) = \frac{\gamma\tilde{n}(s,0) - \dfrac{Un_0}{sD}}{(\gamma+M-N)(\gamma+M+N)} \tag{A15}$$

where

$$M = -\frac{U}{2D}, \tag{A16a}$$

$$N = \left[\frac{s}{D} + \frac{2\kappa U}{b^2 D} + A(s+\kappa_m)^{1/2} + \frac{U^2}{4D^2}\right]^{1/2} \tag{A16b}$$

$$A = \frac{2\theta\mathscr{D}_e^{1/2}}{bD} \tag{A17}$$

Using Laplace transforms from the tabulation of Roberts and Kaufman[33] (p. 189 eqns (77) and (78), yields

$$\tilde{n}(s,x) = \tilde{n}(s,0)$$

$$\times\left[\frac{-(M-N)e^{-(M-N)x}+(M+N)e^{-(M+N)x}}{2N}\right]$$

$$-\frac{Un_0}{sD}\left[\frac{e^{-(M-N)x}-e^{-(M+N)x}}{2N}\right] \tag{A18}$$

Applying boundary condition (A10) in (A18) and taking the limit $x \to \infty$, $\tilde{n}(s,0)$ is evaluated to be

$$\tilde{n}(s,0) = -\frac{Un_0}{sD(M-N)} \tag{A19}$$

and upon substitution into (A18) yields

$$\tilde{n}(s,x) = -\frac{Un_0}{sD}\frac{\exp[-(M+N)x]}{M-N}$$
$$= \frac{\frac{Un_0}{SD}\exp\left[\frac{Ux}{2D}\right]\exp\left[-(s_1+ADs_1^{1/2}+E)^{1/2}\frac{x}{D^{1/2}}\right]}{\left[\frac{U}{2D}+\frac{1}{D^{1/2}}(s_1+ADs_1^{1/2}+E)^{1/2}\right]} \tag{A20}$$

where

$$s_1 = s+\kappa_m, \quad E = \frac{2\kappa U}{b^2}+\frac{U^2}{4D}-\kappa_m \tag{A21a, b}$$

The latter formulation in (A20) is a consequence of employing eqn (A16). Inversion from the Laplace time variable s back to the real time variable t is obtained by introducing the following two functions

$$f(s_1) = \frac{Un_0}{(s_1-\kappa_m)D^{1/2}}\exp\left[\frac{Ux}{2D}\right]$$
$$\times\exp\left[-(s_1+ADs_1^{1/2}+E)^{1/2}\frac{x}{D^{1/2}}\right] \tag{A22}$$

and

$$g(s_1) = \frac{1}{\left[\frac{U}{2D^{1/2}}+(s_1+ADs_1^{1/2}+E)^{1/2}\right]}$$
$$= \frac{1}{F+[(s_1^{1/2}+H)^2+P]^{1/2}} = g^0(s_1^{1/2}) \tag{A23}$$

where the latter equality in the preceding equation is obtained by adding and subtracting $A^2D^2/4$ in the denominator, and making use of the following definitions

$$F = \frac{U}{2D^{1/2}}, \quad H = \frac{AD}{2}, \quad P = E-\frac{A^2D^2}{4} \tag{A24a, b, c}$$

In view of the following identity[37]

$$\int_0^\infty \exp\left[-\eta^2-\frac{L^2}{\eta^2}\right]d\eta = \frac{\pi^{1/2}}{2}\exp[-2L] \tag{A25}$$

(A22) is expressed as

$$f(s_1) = \frac{2Un_0\exp\left[\frac{Ux}{2D}\right]}{(s_1-\kappa_m)(\pi D)^{1/2}}\int_0^\infty \exp\left[-\eta^2-\frac{Ex^2}{4D\eta^2}\right]$$
$$\times\exp\left[-\frac{s_1x^2}{4D\eta^2}\right]\exp\left[-\frac{Ax^2s_1^{1/2}}{4\eta^2}\right]d\eta \tag{A26}$$

Using the appropriate Laplace transform from the tabulation of van Genuchten and Alves[41] (p. 103) in conjunction with the first translation or shifting property $L^{-1}\{e^{-as}F(s)\} = f(t-a)$, where $a \geq 0$ and L^{-1} is the Laplace inverse operator,[36] the inverse of $f(s_1)$ is obtained as

$$f(t) = \frac{2Un_0\exp[B]}{(s_1-\kappa_m)(\pi D)^{1/2}}\int_\ell^\infty \exp\left[-\eta^2-\frac{Ex^2}{4D\eta^2}\right]$$
$$\times\left\{\exp\left[\kappa_m T-\frac{\kappa_m^{1/2}Ax^2}{4\eta^2}\right]\right.$$
$$\times\operatorname{erfc}\left[\frac{Ax^2}{8\eta^2T^{1/2}}-(\kappa_m T)^{1/2}\right]$$
$$+\exp\left[\kappa_m T+\frac{\kappa_m^{1/2}Ax^2}{4\eta^2}\right]$$
$$\left.\times\operatorname{erfc}\left[\frac{Ax^2}{8\eta^2T^{1/2}}+(\kappa_m T)^{1/2}\right]\right\}d\eta \tag{A27}$$

where

$$B = \frac{Ux}{2D} \quad \ell = \frac{x}{2(Dt)^{1/2}} \quad T = t-\frac{x^2}{4D\eta^2} \tag{A28a, b, c}$$

Employing the following Laplace inverse relationship from the tabulation of Roberts and Kaufman[33] (p. 171)

$$L^{-1}\{g^0(s_1^{1/2})\} = \frac{1}{2(\pi t^3)^{1/2}}\int_0^\infty \exp\left[-\frac{\omega^2}{4t}\right]R(\omega)\,\omega d\omega \tag{A29}$$

where

$$R(\omega) = L^{-1}\left\{\frac{1}{F+[(s_2+H)^2+P]^{1/2}}\right\} \tag{A30}$$

and s_2 replaces $s_1^{1/2}$. Using the following shift $s_3 = s_2+H$, the preceding equation can be written as

$$R(\omega) = \exp[-H\omega]L^{-1}\left\{\frac{1}{F+[s_3^2+P]^{1/2}}\right\}$$
$$= \exp[-H\omega]L^{-1}\{g^0([s_3^2+P]^{1/2})\} \tag{A31}$$

From the tabulation of Roberts and Kaufman[33] (p. 172) we can obtain the following Laplace inverse relationship

$$L^{-1}\{g^0([s_3^2+P]^{1/2})\} = Q(\omega)-P^{1/2}\int_0^\omega Q[(\omega^2-\nu^2)^{1/2}]$$

$$\times J_1[P^{1/2}\nu]\,d\nu \tag{A32}$$

where

$$Q(\omega) = L^{-1}\left\{\frac{1}{F+s_4}\right\}$$

and s_4 replaces $(s_3^2+P)^{1/2}$. By using the inverse transform relationship $L^{-1}\{1/(a+s)\} = e^{-at}$ from Laplace transform tables,[33] we get

$$Q(\omega) = \exp[-F\omega] \tag{A33}$$

In view of eqns (A29)–(A33), the final form of $g(t)$ can be written as

$$g(t) = \frac{1}{2(\pi t^3)^{1/2}}\left\{\int_0^\infty \exp\left[-\frac{\omega^2}{4t} - \omega(F+H)\right]\omega\,d\omega - P^{1/2}\int_0^\infty\int_0^\omega \exp\left[-\frac{\omega^2}{4t} - H\omega - F(\omega^2-\nu^2)^{1/2}\right] \times J_1[\nu P^{1/2}]\omega\,d\nu\,d\omega\right\} \tag{A34}$$

Now that $f(t)$ and $g(t)$ are specified, the desired solution is

$$n_{cf_p}(t,x) = \exp[-\kappa_m t][f(t) * g(t)] \tag{A35}$$

where

$$f(t) * g(t) = \int_0^t f(\tau)g(t-\tau)\,d\tau \tag{A36}$$